Aquaporin-4 is removed from the plasma membrane of human Müller cells by AQP4-IgG from NMOSD patients: Changes in cell volume homeostasis as the first step of retinal injury?

Vanina Netti[1], Juan Fernández[1], Luciana Melamud[2], Pablo Garcia-Miranda[3] , Gisela Di Giusto[1], Paula Ford[1], Miriam Echevarria[3] and Claudia Capurro[1#]

[1] *Laboratorio de Biomembranas, Instituto de Fisiología y Biofísica "Bernardo Houssay" (IFIBIO-HOUSSAY), Consejo Nacional de Investigaciones Científicas y Técnicas (CONICET). Departamento de Ciencias Fisiológicas, Facultad de Medicina, Universidad de Buenos Aires, Buenos Aires, Argentina.*

[2] *Consultorio de Neuroinmunología, Centro Universitario de Neurología Dr. J.M. Ramos Mejía, Facultad de Medicina, Universidad de Buenos Aires, Buenos Aires, Argentina.*

[3] *Instituto de Biomedicina de Sevilla (IBiS), Hospital Universitario Virgen del Rocío/CSIC/Universidad de Sevilla, 41013 Seville, Spain.*

[#]**Corresponding author:** Prof. Claudia Capurro, Ph.D. Laboratorio Biomembranas, *IFIBIO Houssay, CONICET-UBA*, Departamento de Ciencias Fisiológicas. Facultad de Medicina, Universidad de Buenos Aires. Paraguay 2155, piso 7 (1121) Buenos Aires, ARGENTINA. TEL: 54-11-59509500 (ext. 2145). e-mail: capurroclaudia@yahoo.com.ar

Running Head: AQP4-IgG affects cell volume regulation in Retinal Müller cells

Precis: AQP4-IgG targets AQP4 affecting the capacity to regulate cell volume after an osmotic swelling (RVD), a key function of Retinal Müller cells.

Key Words: Aquaporin 4; AQP4-IgG; Human Müller Cells; Cell volume regulation

ABSTRACT

Aquaporin-4 (AQP4) is the target of the specific immunoglobulin G autoantibody (AQP4-IgG) produced in patients with neuromyelitis optica spectrum disorders (NMOSD). Previous studies demonstrated that AQP4-IgG binding to astrocytic AQP4 leads to cell-destructive lesions. However, the early physiopathological events in Müller cells in the retina are poorly understood. Here, we investigated the consequences of AQP4-IgG binding to AQP4 of Müller cells, previous to the inflam- matory response, on two of AQP4's key functions, cell volume regulation response (RVD) and cell proliferation, a process closely associated with changes in cell volume. Experiments were performed in a human retinal Müller cell line (MIO-M1) exposed to complement-inactivated sera from healthy volunteers or AQP4-IgG positive NMOSD patients. We evaluated AQP4 expression (immunofluorescence and western blot), water permeability coefficient, RVD, intracellular calcium levels and membrane potential changes during hypotonic shock (fluorescence videomicroscopy) and cell proliferation (cell count and BrdU incorporation). Our results showed that AQP4-IgG binding to AQP4 induces its partial internalization, leading to the decrease of the plasma membrane water permeability, a reduction of swelling-induced increase of intracellular calcium levels and the impairment of RVD in Müller cells. The loss of AQP4 from the plasma membrane induced by AQP4-IgG positive sera delayed Müller cells' proliferation rate. We propose that Müller cell dysfunction after AQP4 removal from the plasma membrane by AQP4-IgG binding could be a non-inflammatory mechanism of retinal injury in vivo, altering cell volume homeostasis and cell proliferation and consequently, contributing to the physiopathology of NMOSD.

Keywords Aquaporin 4 · AQP4-IgG · Human Müller cells · Cell volume regulation · Cell proliferation

1. INTRODUCTION

Neuromyelitis Optica spectrum disorders (NMOSD) is a devastating, inflammatory and demyelinating disease of the central nervous system (CNS) that preferentially affects the optic nerves and spinal cord (*Pittock & Lucchinetti, 2016*). The majority of patients are seropositive for a highly specific serum immunoglobulin G that targets Aquaporin-4 (AQP4), called AQP4-IgG (*Lennon et al., 2004; 2005*). AQP4 is the major plasma membrane water channel in the CNS and it is highly expressed in the polarized plasma membrane of astrocytic endfeet facing the blood-brain barrier as two major isoforms (M1 and M23), which are organized in structures known as orthogonal arrays of particles (OAPs) (*Nagelhus & Ottersen, 2013*). Clinical and pathological studies have proposed that AQP4-IgG binding to astrocytic AQP4 produces complement-dependent cytotoxicity, which leads to astrocyte-destructive lesions in spinal cord and optic nerves (*Bradl et al., 2018; Chang & Chang, 2019*). However, new evidence indicates that AQP4-IgG can also induce complement-independent pathologenesis suggesting that different mechanisms of AQP4-IgG may act concurrently *(Ratelade & Verkman, 2012; Bennet et al, 2017*).

In addition to astrocytes, AQP4 is also highly expressed in Müller cells in the inner retina and in glial membranes contacting retinal ganglion cells as well as in nerve fibers (*Reichenbach & Bringmann, 2020*). Using optical coherence tomography (OCT), several studies demonstrated that damage to optic nerves in NMOSD is also associated with retinal injury (*Gelfand et al., 2013; Sotirchos et al., 2013; Bennett et al., 2015; Peng et al., 2017).* Other reports demonstrate that NMOSD patients AQP4-IgG-seropositive without a history of optic neuritis, have microstructural changes in the fovea region, a retinal site rich in Müller cells, supporting the proposal of Müller cells as a target of AQP4-IgG (*Oertel et al., 2017*). However, until a few years ago there was no direct evidence of retinal lesions in patients with NMOSD (*Zeka et al., 2016*). Intravitreal injection to adult rats retina of a monoclonal AQP4-specific recombinant antibody derived from an NMOSD patient (rAb-53) showed that, in fact, the antibody efficiently bound to AQP4 on retinal Müller cells and produced complement-independent retinal injury (*Felix et al., 2016*). However, as AQP4-IgG is

a polyclonal autoantibody that binds multiple epitopes with variable avidity for them (*Pittock & Lucchinetti, 2016*), the effects of NMOSD patients' sera on Müller cells warrants further study.

One of the major functional roles of Müller cells is to maintain extracellular fluid and ionic homeostasis within the retina, since neural activity alters osmotic gradients leading to cell swelling, which is followed by a regulatory volume decrease (RVD) response, in which AQP4-mediated water transport would play an active role (*Pannicke et al., 2010*). We have previously reported that RVD in Müller cells is a complex response that involves Transient Receptor Potential Vanilloid 4 (TRPV4) calcium channel-dependent changes in membrane potential (Vm) as well as the activation of K^+ and Cl^- channels and the release of amino acids such as Taurine and Glutamate via the Volume Regulated Anion Channel (VRAC) (*Fernández et al., 2013; Netti et al, 2017; Netti et al., 2018*). Even more, Jo et al. (2015) showed that TRPV4 -AQP4 interactions constitute a molecular system that finetune astroglial volume regulation by integrating osmosensing, calcium signaling and water transport, and when over-activated, they can trigger pathological swelling. However, the consequences of AQP4-IgG binding to AQP4 on RVD machinery was not investigated, in particular the putative involvement of TRPV4 in NMOSD physiopathology.

Another important role of Müller cells is to maintain retinal integrity responding to injury by a mechanism known as reactive gliosis, which involves the activation of the cell cycle and subsequent dedifferentiation to other cell types, having a role of stem cells in the adult retina (*Fischer and Reh, 2001; Ooto et al., 2004; Giaume et al., 2007*). Interestingly, stem cell transplantation has been considered to be a potential treatment method for neurological disorders including NMOSD (*Greco et al., 2014*). Since it was proved that AQP4 affects cell proliferation in different cell types (*Kong et al., 2008; Li et al., 2016*) and several AQPs have a role in cell proliferation by allowing fast cell volume regulation during cell division (*Di Giusto et al., 2012; Galán-Cobo et al., 2016*), the aim of this study was to investigate whether binding of AQP4-IgG to AQP4 in Müller cells will threat cell volume regulatory capacity and consequently cell proliferation. We used a human retinal Müller cell line (MIO-M1), a good model that expresses endogenous AQP4 and maintains important functional characteristics of Müller cells (*Limb et al., 2002*) exposed

to AQP4-IgG positive sera from different NMOSD patients. Our results propose that retinal injury may be driven by the dysfunction of Müller cells in patients with AQP4-IgG. Understanding these mechanisms will pave the way for therapeutic interventions in NMOSD.

2. MATERIAL AND METHODS

2.1 Cell Cultures

The MIO-M1 cell line (kindly provided by Dr. Astrid Limb, University College London, London, UK) is a spontaneously immortalized retinal Müller glial cell line, originated from human retina, that retained many characteristics of Müller cells (*Limb et al., 2002*). Cells were grown as monolayers in the presence of Dulbecco's Modified Eagle Medium (DMEM) / glutamax supplemented with 10% fetal calf serum (FCS), with 5 µg/ml streptomycin and 5 U/ml penicillin at 37°C in a humidified atmosphere containing 5% CO_2. Cells were routinely subcultured every week. For immunofluorescence and functional studies, MIO-M1 cells were seeded on glass coverslips (diameter 1.2 cm) at 5-10 x 10^3 cells/ml densities, for 48 hours and then subjected to the different experimental conditions.

2.2 Patients and serum samples

Serum samples were collected from patients that fulfilled the original diagnostic criteria for NMO and were AQP4-IgG positive, as previously described (*Wingerchuk et al., 2015*), from the Neuroimmunologic Clinic Service of the Ramos Mejia Hospital, Argentina and from the Neurology Department at the Virgen of Rocío University Hospital (HUVR), Spain. As control, we included serum from healthy AQP4-IgG negative volunteers. All subjects signed the informed consent form, and the study was approved by the Institutionals Review Boards and conducted in compliance with the Declaration of Helsinki. Demographic and clinical characteristics of patients included in our study were previously reported (*Melamud et al., 2012; García-Miranda et al, 2019*). Sera were stored at -80°C and complement was inactivated holding 30 minutes at 56°C.

2.3 Cells pretreatment with control or patient Sera

MIO-M1 human Müller cells were exposed to control or patients heat-inactivated sera (dilution 1/50 in culture media) for 1 hour at 4°C or 12 hours at 37°C. These conditions were selected to avoid or to facilitate AQP4 down-regulation, respectively, as previously described in HEK-293 cells and astrocytes primary culture (*Melamud et al., 2012; Hinson et al, 2012*). As a control for AQP4 function in Müller cells, in some experiments, cells were preincubated with 100 nM of the specific AQP4 inhibitor N-1,3,4-Thiadiazol-2-yl-3-pyridinecarboxamide (TGN-020, *Kida et al., 2017*) (Sigma-Aldrich) in the isoosmotic extracellular solution and the same concentration was used throughout the experiments. After these treatments, cells were washed with PBS and then immunofluorescence or functional studies were performed.

2.4 Measurement of Cell Volume Changes, Water permeability, RVD Response and intracellular calcium levels

MIO-M1 cells were seeded on glass coverslips (12 mm diameter) at 5-10 x 10^3 cells/mL densities for 48 hours and then subjected to the different experimental conditions. As previously reported, we simultaneously recorded changes in cell volume and intracellular calcium levels ($[Ca^{2+}]_i$) in single cells by using 14 µM of the calcium-sensitive dye Fura-2 AM (Invitrogen, Thermo Fisher Scientific). Cells were incubated for 60 minutes at 37 ºC and then fluorescence was recorded at the calcium-sensitive (380 nm, R_t/R_0 Fura-2) and -insensitive (358 nm, isosbestic) wavelengths with a Nikon TE-200 epifluorescence inverted microscope (Nikon Planfluor 40X oil immersion objective lens), coupled to a device camera (Hamamatsu C4742-95), and connected to a computer with the Metafluor software acquisition program (Universal Imaging Corporation, PA) (*Netti et al., 2017*). Cells were exposed to hypotonic shock and relative fluorescence (F_t/F_0) was recorded. F_0 represents the pinhole signal when placed in equilibrium with an iso-osmotic medium with an osmolality OsM_0 (300 mOsM) and F_t is the fluorescence from the same region at time *t*, when placed in equilibrium with a solution with an osmolality of OsM_t. Changes in cell volume can be calculated as follows:

$$\frac{V}{V_0} = \frac{\left(\frac{F_0}{F_t}\right) - f_b}{1 - f_b}$$

where V is cell volume at time t; V_0 is cell volume at t = 0; and f_b is the relative background. This parameter corresponds to the y intercept of a plot of F_0/F_t versus OsM_0/OsM_t, which represents relative fluorescence in the absence of osmolality changes.

RVD after cell exposure to a hypo-osmotic medium was calculated by the following equation:

$$\%RVD_{20} = \left[\frac{\left(\frac{V}{V_0}\right)_{\max} - \left(\frac{V}{V_0}\right)_{20}}{\left(\frac{V}{V_0}\right)_{\max} - 1}\right] \times 100$$

where $(V/V_0)_{max}$ is the maximal value of V/V_0 attained during hypo-osmotic swelling (peak), and $(V/V_0)_{10}$ represents the value of V/V_0 observed at time 20 min after the osmotic shock. $\%RVD_{20}$ thus denotes the magnitude of volume regulation 20 minutes after the osmotic shock, with 100% RVD indicating complete volume regulation and 0 % RVD indicating no volume regulation.

Osmotic water permeability of MIO-M1 cells was estimated from the time course of V/V_0 during the first 2 minutes. Curves for each experiment were fitted with a single exponential function with the software GraphPad Prism 5.0 and the osmotic water permeability coefficient (P_f), was calculated from the exponential time constant (τ) by the equation:

$$P_f = \frac{V_0}{\tau . A . OsM . V_w}$$

where V_0 is the initial cell water volume; A is the cell surface area; OsM is the osmotic gradient and V_W is the partial molar volume of water (18 cm^3. mol^{-1}). Volume-area relation (V_0/A) of MIO-M1 cells was calculated from confocal images using Imaris 7.1.0 software (Bitplane) with a mean value of 20.85 ± 0.70 ($.10^{-5}$ cm, n = 27).

2.5 Measurement of Membrane Voltage Changes

Transmembrane potential was measured using $DIBAC_4(3)$, a slow response anionic dye whose emission is independent of cell volume changes. Cells were loaded with 2.5 μM $DIBAC_4(3)$ for 15 minutes at 20ºC and placed on the stage of the same microscope described in the previous section. Excitation wavelength was 490 nm and emitted light (above 520 nm) was recorded at 10 second intervals. Fluorescence intensity was monitored until it reached a stable value before starting the experiments. Fluorescence intensity changes after interventions were relativized to stationary values (F_t/F_0) and data were corrected for background noise and drift.

2.6 Immunofluorescence assays and quantification of AQP4

For AQP4 detection, MIO-M1 cells were fixed in 4% paraformaldehyde for 1 hour and then permeabilized with 1% glycine and 0.1% Triton X-100 at room temperature. Samples were blocked with 5% Fetal Bovine Serum for 2 hours and sequentially incubated with a rabbit polyclonal anti-AQP4 antibody (1/1000) directed against an epitope located at the intracellular C-terminal domain of rat AQP4 to amino acid residues 249-323 (#AQP-004, Alomone Labs) overnight at 4°C and a secondary antibody (rabbit anti-Cy3 conjugate, dilution 1:100, Jackson Immuno 111-165-003) for 2 hours at room temperature. Then, nuclei were stained with Hoechst (5 μg/ml) for 1 min. Coverslips were mounted with Vectashield mounting medium. Images were captured using epifluorescence on an Olympus FluoView FV1000 confocal microscope and digitalized. The intensity of AQP4-Cy3 fluorescence was quantified by densitometry using Image-J software and then analyzed using the formula:

$$\sum_{n} IF\ (n)$$

Where *n* stands for the number of optical sections required scanning the entire cell, and IF (n) stands for integrated fluorescence intensity within a given optical section.

To quantify AQP4 at the plasma membrane in MIO-M1 cells, immunofluorescence studies were performed using the same technique but at the beginning, cells were incubated for 30 minutes at 4°C with Alexa Fluor® 488-conjugated wheat germ agglutinin (WGA-488; Thermo Fisher Scientific Cat# W11261) that selectively binds to *N*-acetylglucosamine and *N*-acetylneuraminic acid residues and can be used to label glycoproteins for imaging the plasma membrane in live cells. In other experiments, to evaluate the presence of intracellular AQP4 in early endosomes, double immunostaining was performed by using anti-early endosome antigen 1 (EEA1) mouse monoclonal antibodies (1/300, BD Biosciences) and anti-AQP4 antibodies, as described above. Confocal images were analyzed by using Image J colocalization tools and estimated using the M2 superposition coefficient of Manders (SCM), which measures the fraction of WGA/EEA1 that overlaps AQP4 signal, and is described by the following equation

$$SCM = \frac{\Sigma_i (R_i x G_i)}{\sqrt{\Sigma_i R_i^{\,2} x G_i^{\,2}}}$$

A value of 1 indicates 100% of superposition between signals of colocalized pixels, while a value of 0 indicates absence of colocalization.

For TRPV4 immunostaining, the same protocol was applied and a anti-TRPV4 antibody was used (1/1500; Alomone Labs, #ACC-034). Since plasma membrane TRPV4 expression was low, to identify its presence, we created a mask of plasma membrane as previously described (*Netti et al., 2017*). Briefly, WGA images were binarized so that the signal from WGA was ascribed the value of “1” and the rest of the image was ascribed the value of “0”. The Boolean logical operation “AND” was then performed on the corresponding images, representing signals from TRPV4-Cy3 and from WGA (binary mask). This resulted in generation of a new image (shown in yellow in the figures) in which only the TRPV4-Cy3 fluorescent signal corresponding to the membrane was present.

2.7 Western blotting

Confluent MIO-M1 cells seeded in T25 bottles were washed three times in cold PBS and were incubated for 30 min at 4ºC in RIPA Lysis buffer containing 150 mM NaCl, 50 mM Tris/HCl pH 7.5, 0.5 g % Sodium Deoxycholate, 0.1 g % SDS, 2.5 mM EDTA, 1% Triton 100, 1 mM PMSF, 5 µg/ml aprotinin, 10 µg/ml antipain, 10 µg/ml leupeptin and 10 µg/ml pepstatin. Cells were then collected with a rubber scraper, homogenized and sonicated. Whole cell lysates were obtained by centrifugation at 10,000 g at 4°C for 10 minutes. For plasma membrane enrichment, confluent MIO-M1 cells seeded in T75 bottles were the cells were subjected to the same treatment plus an additional centrifugation was performed at 17,000 g at 4°C for 45 minutes as described by Sachs 2008. Samples were then subjected to electrophoresis in 12% SDS-polyacrylamide gel (Bio-Rad), transferred to a nitrocellulose membrane (Bio-Rad) and blocked 1 hour with 5% non-fat dried skimmed milk. Membranes were then incubated with the rabbit polyclonal anti-AQP4 antibody (1/1000, #AQP-004, Alomone Labs) overnight at 4°C. The blots were then washed and incubated 1 hour at room temperature with an anti-mouse IgG conjugated to horseradish peroxidase (dilution 1:7500, Sigma Aldrich). Membranes were visualized using the chemiluminescence method (SuperSignal Substrate, Pierce) and captured on a Gbox (Syngene).

2.8 Proliferation assays

For cell count, MIO-M1 cells were seeded in a 24-well plate at a concentration of 24,000 cells/ml. Control or AQP4-IgG+ sera were added 24 hours after seeding and these experimental conditions were maintained during the whole experiment. At each experimental time (0 to 72 hours), the cells were harvested by trypsinization, resuspended in Trypan blue to exclude non-viable cells and estimate cell viability, and counted on a hemocytometer (Neubauer chamber). Cell doubling time was obtained after adjusting the results to an exponential function using GraphPad Prism software.

For cell proliferation analysis, MIO-M1 cells were pulsed with 20 mM of the thymidine analog 5-Bromodeoxyuridine (BrdU; Sigma-Aldrich) for 1 h. Cells were fixed in 3%

paraformaldehyde for 30 minutes and then neutralized with NH_4Cl 50 mM/PBS for 15 min. BrdU content was analyzed after DNA denaturation with 2 N HCl and 0.1% Triton X-100 at room temperature, followed by neutralization with 0.1M $Na_2B_4O_7$ pH 8.5. The cells were labeled using specific anti-BrdU monoclonal antibodies (Sigma-Aldrich) and Cy2-conjugated secondary antibodies (Jackson Immuno, Pennsylvania, PA). For PI counter-staining, cells were washed twice with PBS and incubated in the presence of PI (50mg/ml) in PBS for 10 minutes in the dark. The percentage of proliferating cells was calculated from the quantification of the total cells stained with IP (red channel) and the positive BrdU (green channel) using an Olympus IMT-2 inverted microscope and ImageJ software.

2.9 Solutions and Chemicals

For functional experiments cells were first set, for at least 10 minutes, in an external iso-osmotic solution containing (mM): 126 NaCl; 5,5 KCl; 2,5 $CaCl_2$; 1,25 $MgCl_2$; 20 Hepes and 10 Glucose (Osmolarity: 299 ± 2 mOsM). Hypo-osmotic solutions were prepared from iso-osmotic solution by the removal of NaCl to create an osmotic gradient of 100 mOsM. All solutions were titrated to pH 7.40 using NaOH (Sigma-Aldrich), and osmolalities were routinely measured by a pressure vapor osmometer (Wescor). Cells were pre-incubated in an iso-osmotic extracellular solution containing drugs or vehicle (DMSO). 1 mM Fura-2 and 0.6 mM $DIBAC_4(3)$ stock solutions were prepared in DMSO and stored at -20°C until used.

2.10 Statistics

Data were evaluated with either Student´s t-test or one-way analysis of variance (ANOVA) followed by Bonferroni's *post hoc* test for multiple comparisons. Bonferroni correction for multiple comparisons (significance cut-off at α/n, being α the level of significance, usually 0.05, and n the number of hypotheses to be tested) was applied when appropriate. Values are reported as mean ±

SEM, and *n* is either the number of cells evaluated in each condition or the number of experiments. All statistical procedures were performed using GraphPad Prism 6 statistical software package.

3. RESULTS

3.1 Long-term exposure to AQP4-IgG reduces AQP4 plasma membrane expression in Müller cells

We and others have previously reported that long-term exposition to AQP4-IgG positive (AQP4-IgG+) serum induced AQP4 internalization in rat astrocytes (*Melamud et al., 2012; Hindson et al., 2012*). In the present study, we analyzed for the first time the effects of the binding of AQP4-IgG+ serum from NMOSD patients to AQP4 expressed in human Müller cells. For this, MIO-M1 cells were exposed to control or AQP4-IgG+ sera for 1 hour at 4ºC or 12 hours at 37ºC, to avoid or to facilitate AQP4 down-regulation, respectively (*Melamud et al., 2012; Hindson et al., 2012*).

Figure 1A resumes representative confocal immunofluorescence experiments, using a polyclonal anti-AQP4 antibody, showing that after exposure of cells for 1 hour at 4°C to control or AQP4-IgG+ sera, AQP4 remained largely expressed in the cell membrane. In contrast, exposure to AQP4-IgG+ serum for 12 hours at 37ºC reduced the AQP4 signal. **Figure 1B** illustrates the quantification of total AQP4 expression in MIO-M1 cells (plasma and intracellular membranes) after exposition at 37°C for 12 hours to AQP4-IgG+ sera from three different NMOSD patients. It can be observed that after the incubation, a significant reduction of AQP4 expression occurs in comparison to cells exposed to control serum.

To confirm whether AQP4 was in fact removed from the plasma membrane when MIO-M1 cells were exposed to AQP4-IgG+ serum for 12 hours at 37ºC, we studied AQP4 colocalization with the plasma membrane marker WGA by confocal immunofluorescence. As shown in **Figure 2A**, when cells were incubated with control serum, AQP4 was largely expressed at the plasma membrane. However, when exposed to AQP4-IgG+ serum, AQP4 plasma membrane expression was largely reduced, as evidenced by the Mander's overlap coefficient (control serum vs AQP4-

IgG+ serum: 0,677 ± 0,043 vs. 0,349 ± 0,064, *n* = 3-4 experiments, p<0.005). In agreement with this, Western blot analysis revealed that the major band for AQP4 expressed at the plasma membrane of Müller cells (~40 KDa) was significantly reduced after treatment with AQP4-IgG+ serum at 37°C for 12 hours, in comparison to cells exposed to control serum (**Figure 2B**). To confirm that AQP4 is internalized to early endosomes after AQP4-IgG binding in Müller cells, we performed immunolocalization experiments of AQP4 and the early endosome antigen 1 (EEA1), which localizes exclusively to early endosomes and was shown to colocalize with AQP4 in astrocytes (*Hinson et al., 2012*). **Figure 2C** shows an increased localization of AQP4 in early endosomes after exposure to AQP4-IgG+ serum (merge*, indicated by arrows), which was also evidenced by Mander's overlap coefficient (control serum vs AQP4-IgG+ serum: 0,315 ± 0,062 vs. 0,874 ± 0,085, *n* = 3 experiments, p<0.01).

Altogether, these results support the partial internalization of AQP4 expressed in the plasma membrane of Müller cells into the endosomal compartment following long-term exposure to AQP4-IgG+ sera.

3.2. AQP4 internalization by long-term exposure to AQP4-IgG reduces Müller cells water permeability and RVD capacity

We next investigated the functional consequences of Müller cells' treatment with control or NMOSD patients´sera for 1 hour at 4°C or 12 hours at 37°C. For this purpose, we measured the time course of MIO-M1 cell swelling (V/V_0) in response to an osmotic gradient (ΔOsM: 100 mOsM) by fluorescence videomicroscopy using FURA-2 AM. **Figure 3A** shows a similar swelling kinetics of V/V_0 in cells exposed to control or AQP4-IgG+ sera for 1 hour at 4°C, without differences in osmotic water permeabilities (Pf, Insert), demonstrating that the binding of AQP4-IgG to AQP4 does not directly inhibit water channel function. The lack of ability of AQP4-IgG+ serum to inhibit water permeability was further demonstrated comparing these results with those obtained by using the novel specific AQP4 inhibitor TGN-020. Our results showed that when AQP4 expressed in Müller cells is blocked with 100 nM TGN-020, Pf was significantly reduced (**Figure 3C**). In contrast,

Figure 3B shows that exposure of Müller cells to AQP4-IgG+ serum for 12 hours at 37°C significantly delayed cell swelling kinetics, as compared to control serum, which can be explained by a reduction of the osmotic water permeability (Insert). In addition, **Figure 3D** shows the percentage of RVD response 15 minutes after the hypotonic shock ($RVD_{15\ min}$) in the three experimental conditions previously described. The % $RVD_{15\ min}$ was comparable between cells exposed to control or AQP4-IgG+ sera for 1 hour at 4°C. However, the capacity of Müller cells to regulate its volume after an osmotic swelling was significantly decreased after exposure for 12 hours at 37°C to AQP4-IgG as compared to control serum, as well as by TGN-020 treatment as compared to vehicle.

We have previously reported that the magnitude of changes in intracellular calcium levels after cell swelling determine the efficiency of RVD in Müller cells (*Netti et al., 2017*). Then, we next evaluated the time course of relative changes in calcium levels (Rt/R_0 Fura-2 AM), during a hypoosmotic shock in cells exposed for 12 hours at 37°C to control or AQP4-IgG positive sera. It can be observed that, in cells treated with AQP4-IgG+ sera, the cell swelling-induced increase in calcium levels was reduced and delayed as compared to control sera (**Figure 4 A, C, D**). Similar results were obtained by blocking AQP4 with TGN-020, which also provoked a decrease of the swelling-induced calcium maximal levels and increased time to peak (**Figure 4B, C, D**). However, no differences were observed in hypotonicity-induced changes in calcium levels of MIO-M1 cells exposed to control or AQP4-IgG+ sera for 1 hour at 4°C (data not shown).

Altogether, these results strongly suggest that AQP4-IgG does not impair AQP4 function as a water channel, but causes its internalization with the consequent reduction of water permeability and the efficiency of the RVD response in Müller cells.

3.3. TRPV4 activity is not affected by AQP4-IgG in Müller cells

We have previously reported that the calcium channel TRPV4 modulates the changes in Vm occurring during RVD (*Netti et al., 2017*). These evidence, together with the demonstration that

TRPV4 and AQP4 channels synergistically regulate cell volume in retinal Müller glia (*Jo et al. 2015*), led us to investigated if the endocytosis of AQP4 by AQP4-IgG+ may also affect TRPV4 activity in Müller cells. For this, MIO-M1 cells were exposed to control or AQP4-IgG+ sera for 12 hours at 37°C and then Vm and TRPV4 expression and activity were measured. Regarding changes in Vm occurring during cell swelling and RVD by videomicroscopy using $DIBAC_4(3)$ (F_t/F_0), we observed that Vm was not affected by AQP4-IgG+ sera as compared with control sera (**Figure 5A**). **Figure 5B** confirms that the expression of TRPV4 was unaffected after exposure to AQP4-IgG+ sera for 12 hours at 37°C. In fact, using an anti-TRPV4 antibody (red) and the plasma membrane marker WGA (green), we observed no changes in colocalized plasma membrane signals (yellow). In addition, we tested TRPV4 function by its activation with the specific agonist 4α-PDD (10 µM) in isotonic conditions. **Figure 5C** shows the kinetics of intracellular calcium levels, where the percentage of responding cells (~50% in each condition) exhibited a similar time to peak (control: 12.9 ± 1.3 vs. AQP4-IgG+: 10.0 ± 1.5 min, n= 25-30 cells of 4-5 experiments, ns) and maximal increase in calcium levels (control: 72.2 ± 8.6 vs. AQP4-IgG+:60.4 ± 6.5 min, n= 25-30 cells of 4-5 experiments, ns). These results strongly suggest that TRPV4 activity/expression is not impaired by AQP4-IgG+ sera in Müller cells.

3.4 Cell proliferation is affected by long-term exposure to AQP4-IgG

We next evaluated if the observed RVD impairment due to AQP4-IgG binding to AQP4 may affect cell proliferation, a process strictly associated with cell volume changes. For this, we first evaluated the kinetics of cell growth in MIO-M1 cells after incubation up to 72 hours with control or AQP4-IgG+ sera from three different patients. It can be noticed that the cells exposed to AQP4-IgG+ decreased their rate of growth in comparison to those exposed to the control sera, which is reflected by a significant increase in the period of time required for cells to double in number (**Figure 6A and B**). Similar results were obtained when MIO-M1 cells were incubated with the inhibitor TGN-020, demonstrating that AQP4 is involved in the proliferation of Müller cells, as previously shown in other cell types (**Figure 6B**). Importantly, these changes in cell growth are not

due to cell death since cell viability, assessed by Trypan Blue exclusion method, was not affected by the presence of AQP4-IgG as compared to the control sera or in the presence of TGN-020 (data not shown).

We further evaluated MIO-M1 cell proliferation in the presence of control or AQP4-IgG+ sera by measuring the incorporation of the thymidine analog 5-Bromodeoxyuridin (BrdU) as a marker of DNA synthesis and calculated the percentage of proliferating cells. Results showed that BrdU positive cells ($BrdU^+$) are reduced in the presence of AQP4-IgG, as compared to control serum (**Figure 6C**). Quantification of the total number of $BrdU^+$ cells effectively demonstrated that the percentage of proliferative cells is significantly reduced with the AQP4-IgG^+ sera from the three patients (**Figure 6D**). As expected, pretreatement of MIO-M1 cells with TGN-020 showed a similar reduction of BrdU incorporation. These results demonstrate that before complement activation, AQP4 loss from the plasma membrane altered the capacity of Müller cells to proliferate, probably having an impact on retinal tissue repair *in vivo*.

4. DISCUSSION

In the present work, we confirm that AQP4 expressed in human retinal Müller cells represents a pathogenic ocular target of AQP4-IgG, as previously suggested by clinical observations and *in vitro* animal models (*Gelfand et al., 2012; Sotirchos et al., 2012; Green et al., 2009; Levin et al., 2013).* One of the main findings of this study is that the auto-antibody binding to AQP4, before complement activation, does not directly inhibit AQP4 water permeability by blocking the water pore, but induces its partial internalization. In fact, we showed that, under conditions where membrane fluidity and metabolic processes are restricted (4°C for 1 hour), AQP4 remains in the plasma membrane and its water channel activity is not affected. This was further confirmed by comparing these results with those obtained by the use of TGN-020 inhibitor, which specifically blocks the AQP4 pore as shown by molecular dynamics studies (*Toft-Bertelsen et al. 2020*). The long-term exposure to AQP4-IgG+ sera for 12 h at 37°C, a condition that does not prevent

metabolic processes, reduced AQP4 expression and induced its partial removal of the plasma membrane to the endosomal compartment. AQP4 down-regulation induced by AQP4-IgG+ sera in Müller cells is in line with the report of *Felix et al.* (2016) using a monoclonal antibody, as well as with our and other previous reports in astrocytes (*Melamud et al., 2012; Hindson et al., 2012*). In fact, these studies showed that while AQP4-IgG+ sera induced the endocytosis of M1 isoform in astrocytes, M23 still remain in the plasma membrane, rearranging to larger OAPs. However, several other AQP4 isoforms were later described, produced by alternative splicing (AQP4b, d, e and f) or by translational readthrough that contains a C-terminal extension (AQP4ex) (*De Bellis et al., 2017; Lisjak et al., 2020*). It was proposed that AQP4ex could have an important regulatory role in OAP assembly and stability, being critical for the binding of pathogenic human AQP4-IgG autoantibodies in astrocytes (*Palazzo et al., 2019*). In the present study, Western blot analysis for AQP4 revealed that human Müller cells express several isoforms, but the major band observed at the plasma membrane, which was partially removed after AQP4-IgG binding, is that of ~40 kDa, which may correspond to AQP4-ex. However, we cannot discard that the AQP4e isoform, a protein of also ~40 kDa present in the plasma membrane and participating in the cell volume regulation of astrocytes (*Lisjak et al., 2017*), could be also involved. The present study does not attempt to clarify this point; however, our observations support the idea that, in human Müller cells, AQP4-IgG would not bind to the canonical M1 and M23 isoforms. Future studies are needed to address this novel issue since, as previously reported, the expression of particular AQP4 isoforms depend mainly on post-transcriptional regulation, according to the specific homeostatic needs of each tissue (*Palazzo et al, 2019*).

The here observed endocytosis of AQP4 by AQP4-IgG is functionally relevant, since it leads to the decrease of plasma membrane water permeability and the impairement of one of the major roles of Müller cells, the control of the RVD response. In fact, after the partial removal of AQP4 by AQP4-IgG, the changes of intracellular calcium levels, which determine the efficiency of RVD mechanisms (*Netti et al., 2017*), were also significantly reduced. These results propose an association between the presence of AQP4 and the osmotically-induced calcium signals in Müller

cells, as previously shown in astrocytes (*Thrane et al., 2011*), which is probably altered in the presence of AQP4-IgG, affecting cell volume regulation response. Interestingly, AQP4-IgG does not affect neither TRPV4 expression/activity nor Vm changes occurring during cell swelling and RVD in Müller cells, indicating that AQP4 is the main contributor to the RVD response. This was further confirmed with the specific blocker of the pore of AQP4 by TGN-020. We propose that the activation of RVD effectors would be sensitive to the dynamics of cell swelling and/or its consequences (changes in membrane tension, dilution of intracellular mediators, etc), as previously reported for some AQPs (*Galizia et al., 2008; Di Giusto et al., 2012*). Therefore, the rapid influx of water in the presence of AQP4 will lead to a faster regulation of cell volume changes by activating AQP4-dependent cell volume regulation machinery, as previously shown in mouse-cultured glial cells (*Mola et al., 2016*).

Previous reports in mouse Müller cells described that AQP4 deletion is associated with reactive gliosis and gliovascular modifications which involves the activation of the cell cycle and cell differentiation (*Nicchia et al., 2016*). We here provide experimental evidence demonstrating, for the first time, that before complement activation, the loss of AQP4 from the plasma membrane induced by AQP4-IgG+ sera delayed the ability of Müller cells to proliferate. We also show that AQP4 inhibition with TGN-020 effectivelly reduced the proliferation of Müller cells without inducing cell death, directly demonstrating the contribution of AQP4 to this process. These results are in agreement with our and other studies in different cell types demonstrating that AQPs play a key role in cell volume control, an important prerequisite for the regulation of various cell properties, including proliferation, migration and differentiation *(Galán-Cobo et al., 2016; Di Giusto et al., 2012).* Even more, it was previously reported that AQP4 has a crucial role in regulating proliferation and differentiation of adult neural stem cells by its action on intracellular calcium dynamics (*Kong et al., 2008*) . We here show that the blockage or endocytosis of AQP4, with TGN-020 and AQP4-IgG respectively, not only altered intracellular calcium levels during the osmotic swelling and RVD but also delayed cell proliferation. Therefore, we propose that AQP4-mediated rapid changes in cell volume and in calcium signals facilitate cell proliferation in physiological conditions. Shedding

light on how AQP4 is able to regulate Müller cells proliferation can increase our knowledge of their biological behaviours and improve their application in regenerative and reparative medicine for NMOSD patients. Interenstingly, recent reports revealed that bone marrow mesenchymal stem cells derived from patients with NMOSD exhibited a decreased proliferation rate, together with a decreased expression of several cell cycle promoting and proliferation-associated genes, as compared to control healthy donors (*Yang et al., 2019*). The key role of AQP4 on cell proliferation might also explain the *in vivo* reported structural and functional Müller cells' dysfunction observed, by full-field electroretinography and spectral-domain OCT, only in NMOSD patients who were AQP4-IgG positive (*You et al. 2019*). Further studies are warranted to investigate these mechanisms and its potential implications for the prognosis and treatment of optic neuritis in NMOSD.

In conclusion, we here propose that AQP4-IgG present in the sera of NMOSD patients causes the removal of endogenously expressed AQP4 from the plasma membrane of retinal Müller cells, affecting osmotic water permeability, the consequent activation of the cell volume regulation machinery and cell proliferation. Since all experiments were performed in the absence of complement activation, we can hypothesize that AQP4 removal from the plasma membrane by AQP4-IgG binding could be the first step of retinal injury *in vivo*, altering cell volume homeostasis and retinal regeneration of Müller cells, contributing to the physiopathology of NMOSD.

Acknowledgments

The authors thank Dr. Astrid Limb (University College London, London, UK) for providing the human Müller Cell Line (MIO-M1) and Ricardo Dorr and Teresa Politi for technical assistance.

References

1. Pittock SJ, Lucchinetti CF. Neuromyelitis optica and the evolving spectrum of autoimmune aquaporin-4 channelopathies: a decade later. Ann N Y Acad Sci. 2016;1366(1):20-39. doi:10.1111/nyas.12794

2. Lennon VA, Wingerchuk DM, Kryzer TJ, Pittock SJ, Lucchinetti CF, Fujihara K, Nakashima I, Weinshenker BG. A serum autoantibody marker of neuromyelitis optica: distinction from multiple sclerosis. Lancet. 2004; 364: 2106-2112.
3. Lennon VA, Kryzer TJ, Pittock SJ, Verkman AS, Hinson SR. IgG marker of optic-spinal multiple sclerosis binds to the aquaporin-4 water channel. J Exp Med. 2005; 202: 473-477.
4. Nagelhus EA, Ottersen OP. Physiological roles of aquaporin-4 in brain. Physiol Rev. 2013 Oct;93(4):1543-62. doi: 10.1152/physrev.00011.2013.
5. Bradl M, Reindl M, Lassmann H. Mechanisms for lesion localization in neuromyelitis optica spectrum disorders. Curr Opin Neurol. 2018;31(3):325-333. doi:10.1097/WCO.0000000000000551
6. Chang VTW, Chang HM. Review: Recent advances in the understanding of the pathophysiology of neuromyelitis optica spectrum disorder. Neuropathol Appl Neurobiol. 2020;46(3):199-218. doi:10.1111/nan.12574
7. Ratelade J, Verkman AS. Neuromyelitis optica: aquaporin-4 based pathogenesis mechanisms and new therapies. Int J Biochem Cell Biol. 2012; 44: 1519-1530.
8. Bennett JL, Owens GP. Neuromyelitis Optica: Deciphering a Complex Immune-Mediated Astrocytopathy. J Neuroophthalmol. 2017;37(3):291-299. doi:10.1097/WNO.0000000000000508
9. Reichenbach A, Bringmann A. Glia of the human retina. Glia. 2020;68(4):768-796. doi:10.1002/glia.23727
10. Gelfand JM, Cree BA, Nolan R, Arnow S, Green AJ. Microcystic inner nuclear layer abnormalities and neuromyelitis optica. JAMA Neurology. 2013; 70: 629-633.
11. Sotirchos ES, Saidha S, Byraiah G, Mealy MA, Ibrahim MA, Sepah YJ, Newsome SD, Ratchford JN, Frohman EM, Balcer LJ, Crainiceanu CM, Nguyen QD, Levy M, Calabresi PA. In vivo identification of morphologic retinal abnormalities in neuromyelitis optica. Neurology. 2013; 80(15):1406-14.
12. Bennett JL, de Seze J, Lana-Peixoto M, et al. Neuromyelitis optica and multiple sclerosis: Seeing differences through optical coherence tomography. Mult Scler. 2015;21(6):678-688. doi:10.1177/1352458514567216
13. Peng C, Wang W, Xu Q, et al. Structural Alterations of Segmented Macular Inner Layers in Aquaporin4-Antibody-Positive Optic Neuritis Patients in a Chinese Population. PLoS One. 2016;11(6):e0157645. doi:10.1371/journal.pone.0157645
14. Oertel FC, Kuchling J, Zimmermann H, et al. Microstructural visual system changes in AQP4-antibody-seropositive NMOSD. Neurol Neuroimmunol Neuroinflamm. 2017;4(3):e334. doi:10.1212/NXI.0000000000000334
15. Zeka B, Hastermann M, Kaufmann N, et al. Aquaporin 4-specific T cells and NMO-IgG cause primary retinal damage in experimental NMO/SD. Acta Neuropathol Commun. 2016;4(1):82. doi:10.1186/s40478-016-0355-y
16. Felix CM, Levin MH, Verkman AS. Complement-independent retinal pathology produced by intravitreal injection of neuromyelitis optica immunoglobulin G. J Neuroinflammation. 2016;13(1):275. doi:10.1186/s12974-016-0746-9
17. Pannicke T, Wurm A, Iandiev I, Hollborn M, Linnertz R, Binder DK, Kohen L, Wiedemann P, Steinhäuser C, Reichenbach A, Bringmann A. Deletion of aquaporin-4 renders retinal glial cells more susceptible to osmotic stress. J Neurosci Res. 2010; 88: 2877-2888.
18. Fernández JM, Di Giusto G, Kalstein M, et al. Cell volume regulation in cultured human retinal Müller cells is associated with changes in transmembrane potential. PLoS One. 2013;8(2):e57268. doi:10.1371/journal.pone.0057268
19. Netti V, Fernández J, Kalstein M, et al. TRPV4 Contributes to Resting Membrane Potential in Retinal Müller Cells: Implications in Cell Volume Regulation. J Cell Biochem. 2017;118(8):2302-2313. doi:10.1002/jcb.25884
20. Netti V, Pizzoni A, Pérez-Domínguez M, et al. Release of taurine and glutamate contributes to cell volume regulation in human retinal Müller cells: differences in modulation by calcium. J Neurophysiol. 2018;120(3):973-984. doi:10.1152/jn.00725.2017

21. Jo AO, Ryskamp DA, Phuong TT, et al. TRPV4 and AQP4 Channels Synergistically Regulate Cell Volume and Calcium Homeostasis in Retinal Müller Glia. J2015;35(39):13525-13537. doi:10.1523/JNEUROSCI.1987-15.2015
22. Fischer, A., Reh, T. Müller glia are a potential source of neural regeneration in the postnatal chicken retina. Nat Neurosci 4, 247–252 (2001). doi:10.1038/85090
23. Ooto S, Akagi T, Kageyama R, et al. Potential for neural regeneration after neurotoxic injury in the adult mammalian retina. Proc Natl Acad Sci U S A. 2004;101(37):13654-13659. doi:10.1073/pnas.0402129101
24. Giaume, C., Kirchhoff, F., Matute, C. et al. Glia: the fulcrum of brain diseases. Cell Death Differ 14, 1324–1335 (2007). doi:10.1038/sj.cdd.4402144
25. Greco R, Bondanza A, Vago L, et al. Allogeneic hematopoietic stem cell transplantation for neuromyelitis optica. Ann Neurol. 2014;75(3):447-453. doi:10.1002/ana.24079
26. Kong H, Fan Y, Xie J, et al. AQP4 knockout impairs proliferation, migration and neuronal differentiation of adult neural stem cells. J Cell Sci. 2008;121(Pt 24):4029-4036. doi:10.1242/jcs.035758
27. Li YB, Sun SR, Han XH. Down-regulation of AQP4 Inhibits Proliferation, Migration and Invasion of Human Breast Cancer Cells. Folia Biol (Praha). 2016;62(3):131-137.
28. Di Giusto G, Flamenco P, Rivarola V, et al. Aquaporin 2-increased renal cell proliferation is associated with cell volume regulation. J Cell Biochem. 2012;113(12):3721-3729. doi:10.1002/jcb.24246
29. Galán-Cobo A, Ramírez-Lorca R, Echevarría M. Role of aquaporins in cell proliferation: What else beyond water permeability?. Channels (Austin). 2016;10(3):185-201. doi:10.1080/19336950.2016.1139250
30. Limb GA, Salt TE, Munro PM, Moss SE, Khaw PT. In vitro characterization of a spontaneously immortalized human Muller cell line (MIO-M1). Invest Ophthalmol Vis Sci. 2002; 43: 864-869.
31. Wingerchuk DM et al. International consensus diagnostic criteria for neuromyelitis optica spectrum disorders. Neurology 2015; 85:177-189.
32. Melamud L, Fernandez JM, Rivarola V, Di Giusto G, Ford P, Villa A, Capurro C. Neuromyelitis Optica Immunoglobulin G present in sera from neuromyelitis optica patients affects aquaporin-4 expression and water permeability of the astrocyte plasma membrane. J Neurosci Res. 2012; 90: 1240-1248.
33. García-Miranda P, Morón-Civanto FJ, Martínez-Olivo MDM, Suárez-Luna N, Ramírez-Lorca R, Lebrato-Hernández L, Lamas-Pérez R, Navarro G, Abril-Jaramillo J, García-Sánchez MI, Casado-Chocán JL, Uclés-Sánchez AJ, Romera M, Echevarría M, Díaz-Sánchez M. Predictive Value of Serum Antibodies and Point Mutations of AQP4, AQP1 and MOG in A Cohort of Spanish Patients with Neuromyelitis Optica Spectrum Disorders. Int J Mol Sci. 2019;20(22):5810. Published 2019 Nov 19. doi:10.3390/ijms20225810
34. Hinson SR, Pittock SJ, Lucchinetti CF, Roemer SF, Fryer JP, Kryzer TJ, Lennon VA. Pathogenic potential of IgG binding to water channel extracellular domain in neuromyelitis optica. Neurology. 2007;11; 69: 2221-2231.
35. Kida T, Oku H, Horie T, et al. Implication of VEGF and aquaporin 4 mediating Müller cell swelling to diabetic retinal edema. Graefes Arch Clin Exp Ophthalmol. 2017;255(6):1149-1157. doi:10.1007/s00417-017-3631-z
36. Hinson SR, Romero MF, Popescu BF, et al. Molecular outcomes of neuromyelitis optica (NMO)-IgG binding to aquaporin-4 in astrocytes. Proc Natl Acad Sci U S A. 2012;109(4):1245-1250. doi:10.1073/pnas.1109980108
37. Green AJ, Cree BA. Distinctive retinal nerve fibre layer and vascular changes in neuromyelitis optica following optic neuritis. J Neurol Neurosurg Psychiatry. 2009 Sep;80(9):1002-5. doi: 10.1136/jnnp.2008.166207. Epub 2009 May 21. PMID: 19465415.
38. Levin MH, Bennett JL, Verkman AS. Optic neuritis in neuromyelitis optica. Prog Retin Eye Res. 2013 Sep;36:159-71. doi: 10.1016/j.preteyeres.2013.03.001. Epub 2013 Mar 30. PMID: 23545439; PMCID: PMC3770284.
39. Toft-Bertelsen TL, Larsen BR, Christensen SK, Khandelia H, Waagepetersen HS, MacAulay N. Clearance of activity-evoked K+ transients and associated glia cell swelling occur independently of

AQP4: A study with an isoform-selective AQP4 inhibitor. Glia. 2020;10.1002/glia.23851. doi:10.1002/glia.23851
40. De Bellis M, Pisani F, Mola MG, et al. Translational readthrough generates new astrocyte AQP4 isoforms that modulate supramolecular clustering, glial endfeet localization, and water transport. Glia. 2017;65(5):790-803. doi:10.1002/glia.23126
41. Palazzo C, Buccoliero C, Mola MG, et al. AQP4ex is crucial for the anchoring of AQP4 at the astrocyte end-feet and for neuromyelitis optica antibody binding. Acta Neuropathol Commun. 2019;7(1):51. Published 2019 Apr 1. doi:10.1186/s40478-019-0707-5
42. Lisjak M, Potokar M, Zorec R, Jorgačevski J. Indirect Role of AQP4b and AQP4d Isoforms in Dynamics of Astrocyte Volume and Orthogonal Arrays of Particles. Cells. 2020 Mar 17;9(3):735. doi: 10.3390/cells9030735.
43. Lisjak M, Potokar M, Rituper B, Jorgačevski J, Zorec R. AQP4e-Based Orthogonal Arrays Regulate Rapid Cell Volume Changes in Astrocytes. J Neurosci. 2017 Nov 1;37(44):10748-10756. doi: 10.1523/JNEUROSCI.0776-17.2017.
44. Thrane AS, Rappold PM, Fujita T, et al. Critical role of aquaporin-4 (AQP4) in astrocytic Ca2+ signaling events elicited by cerebral edema. Proc Natl Acad Sci U S A. 2011;108(2):846-851. doi:10.1073/pnas.1015217108
45. Galizia L, Flamenco MP, Rivarola V, Capurro C, Ford P. Role of AQP2 in activation of calcium entry by hypotonicity: implications in cell volume regulation. Am J Physiol Renal Physiol. 2008;294(3):F582-F590. doi:10.1152/ajprenal.00427.2007
46. Nicchia GP, Pisani F, Simone L, et al. Glio-vascular modifications caused by Aquaporin-4 deletion in the mouse retina. Exp Eye Res. 2016;146:259-268. doi:10.1016/j.exer.2016.03.019
47. Thrane AS, Rappold PM, Fujita T, et al. Critical role of aquaporin-4 (AQP4) in astrocytic Ca2+ signaling events elicited by cerebral edema. Proc Natl Acad Sci U S A. 2011;108(2):846-851. doi:10.1073/pnas.1015217108
48. Mola MG, Sparaneo A, Gargano CD, et al. The speed of swelling kinetics modulates cell volume regulation and calcium signaling in astrocytes: A different point of view on the role of aquaporins. Glia. 2016;64(1):139-154. doi:10.1002/glia.22921
49. You Y, Zhu L, Zhang T, et al. Evidence of Müller Glial Dysfunction in Patients with Aquaporin-4 Immunoglobulin G-Positive Neuromyelitis Optica Spectrum Disorder. Ophthalmology. 2019;126(6):801-810. doi:10.1016/j.ophtha.2019.01.016
50. Yang C, Yang Y, Ma L, et al. Study of the cytological features of bone marrow mesenchymal stem cells from patients with neuromyelitis optica. Int J Mol Med. 2019;43(3):1395-1405. doi:10.3892/ijmm.2019.4056

Figure 1

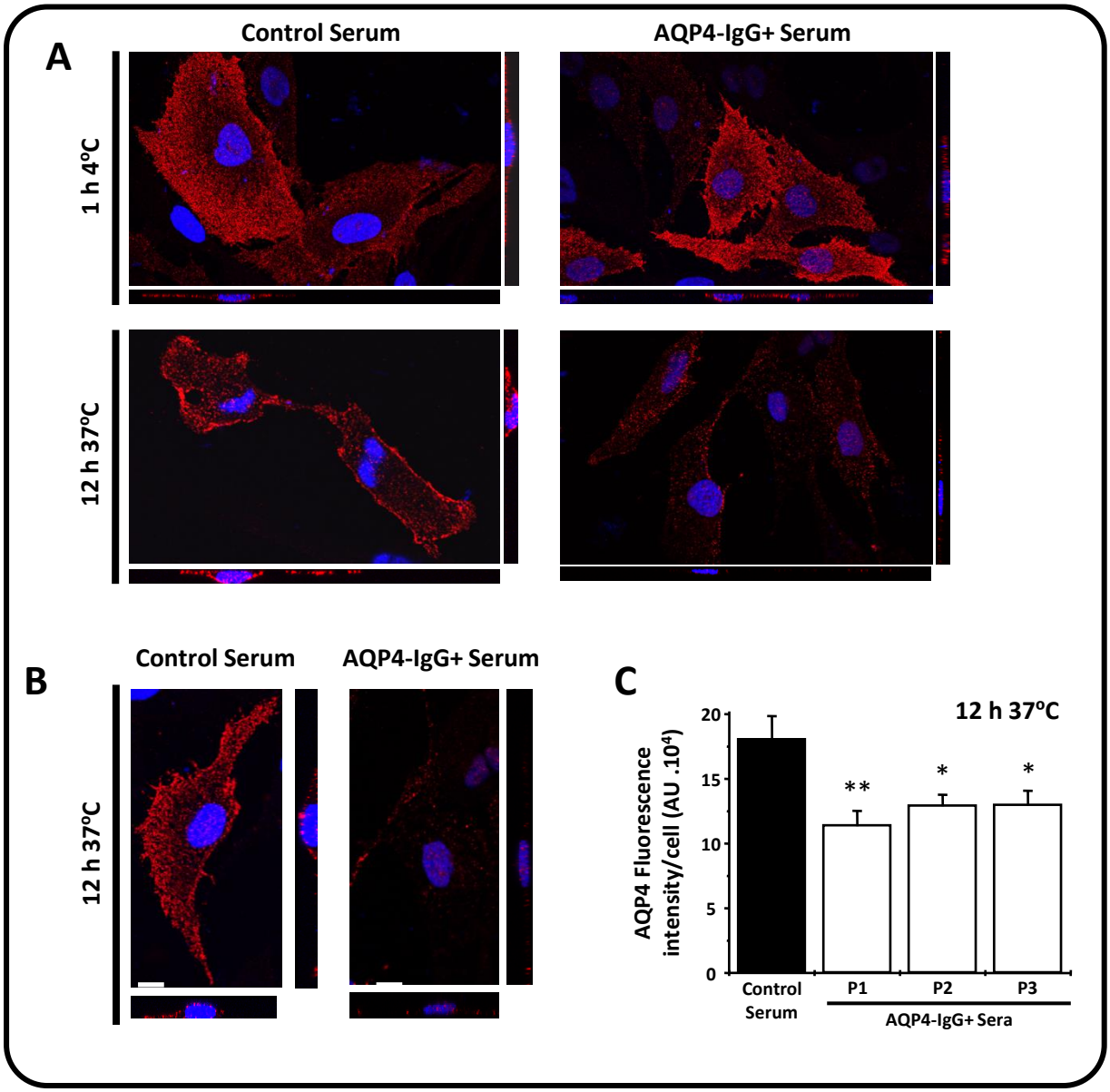

Figure 1: AQP4 expression in MIO-M1 cells after exposure to control or AQP4-IgG positive sera. **A:** Cells were treated for 1 hour at 4°C or 12 hours at 37°C with control or AQP4-IgG+ sera and then immunofluorescence were performed using a polyclonal anti-AQP4 antibody (red). Top panel: Confocal images illustrating similar staining pattern of plasma membrane AQP4 after exposure to control or AQP4-IgG+ sera for 1 hour at 4°C. Lower panel: Confocal images illustrating changes in the staining pattern after exposure for 12 hours at 37°C to AQP4-IgG+ serum, as compared to control serum. Images are representative of three independent experiments. **B:** Detailed magnification of cells exposed to control or AQP4-IgG+ sera for 12 hours at 37°C (Scale bars: 10 µm). **C:** Total fluorescence quantification of positively-stained cells after incubation for 12 hours at 37°C with control or 3 different AQP4-IgG+ sera exposure. Immunofluorescence values per cell (AU: arbitrary units) are expressed as mean ± SEM for 23 - 52 cells from 3 experiments for each condition **p<0.01 and *p<0.05 control vs. AQP4-IgG+ sera.

Figure 2

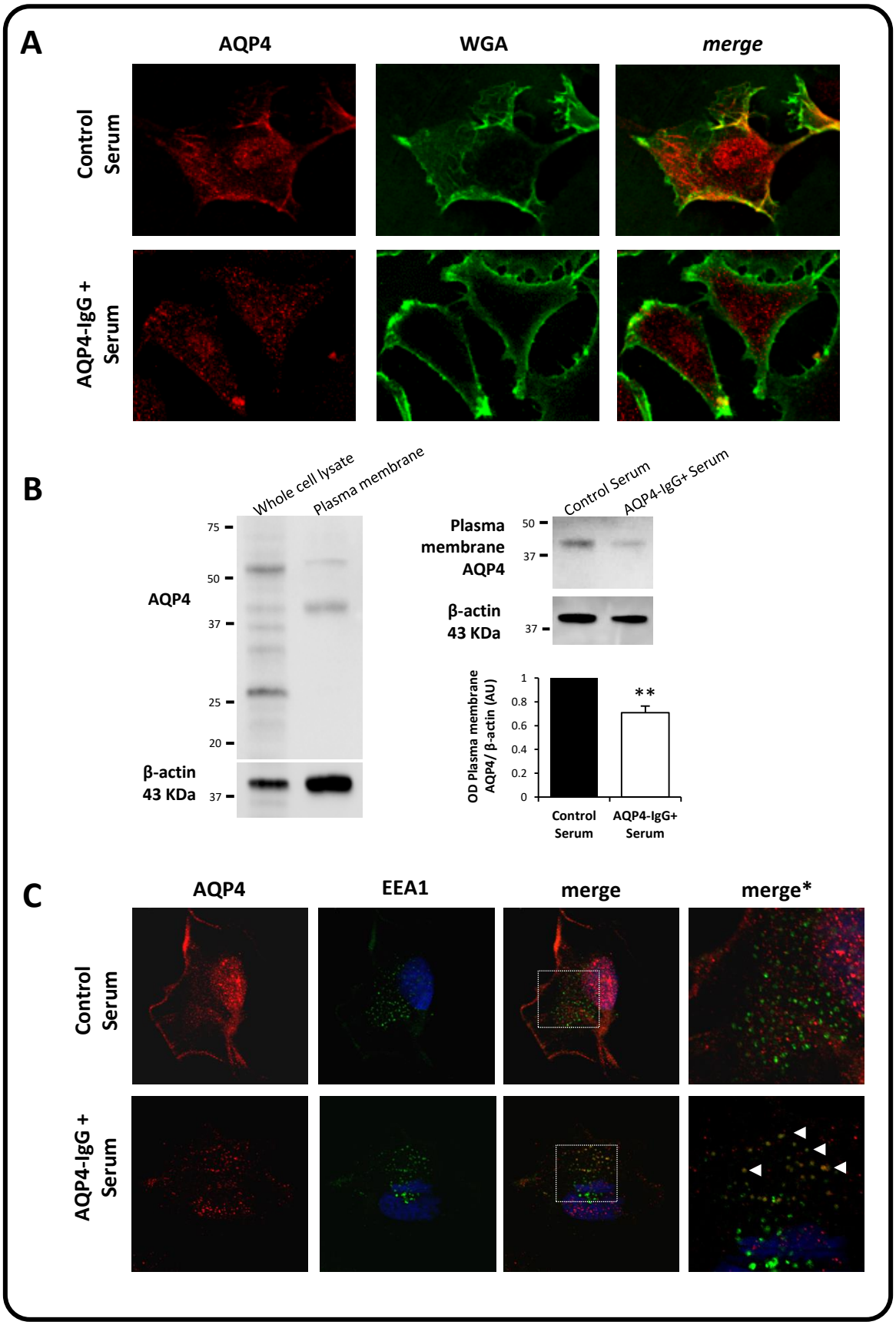
A
AQP4
WGA
merge
Control Serum
AQP4-IgG + Serum
B
Whole cell lysate
Plasma membrane
75
50
37
25
20
AQP4
β-actin 43 KDa
37
Control Serum
AQP4-IgG+ Serum
Plasma membrane AQP4
50
37
β-actin 43 KDa
37
OD Plasma membrane AQP4/ β-actin (AU)
1
0.8
0.6
0.4
0.2
0
**
Control Serum
AQP4-IgG+ Serum
C
AQP4
EEA1
merge
merge*
Control Serum
AQP4-IgG + Serum

Figure 2: AQP4 expression and localization in plasma membrane of MIO-M1 cells after exposure to control or AQP4-IgG positive sera.

A: Immunoflurescence confocal images of MIO-M1 cells (40X) stained with a polyclonal anti-AQP4 antibody (red), WGA plasma membrane staining (green) and merge of both images (yellow) after treatment for 12 hours at 37°C with control (left) or AQP4-IgG sera (right). Images are representative of three independent experiments (Scale bars: 20 μm). **B:** Western blot showing the expression of several AQP4 isoforms in whole cell lysates and in enriched plasma membrane fractions (left) and AQP4 plasma membrane expression after treatment for 12 hours at 37°C with control or AQP4-IgG sera (right). Values are expressed as mean ± SEM, **p<0.005 control vs. AQP4-IgG positive sera. **C:** Immunoflurescence confocal images of MIO-M1 cells (60X) stained with a polyclonal anti-AQP4 antibody (red), EEA1 (green) and merge of both images (yellow) after treatment for 12 hours at 37°C with control (left) or AQP4-IgG sera (right). Merge* show enlarged boxed areas from merged image.

Figure 3

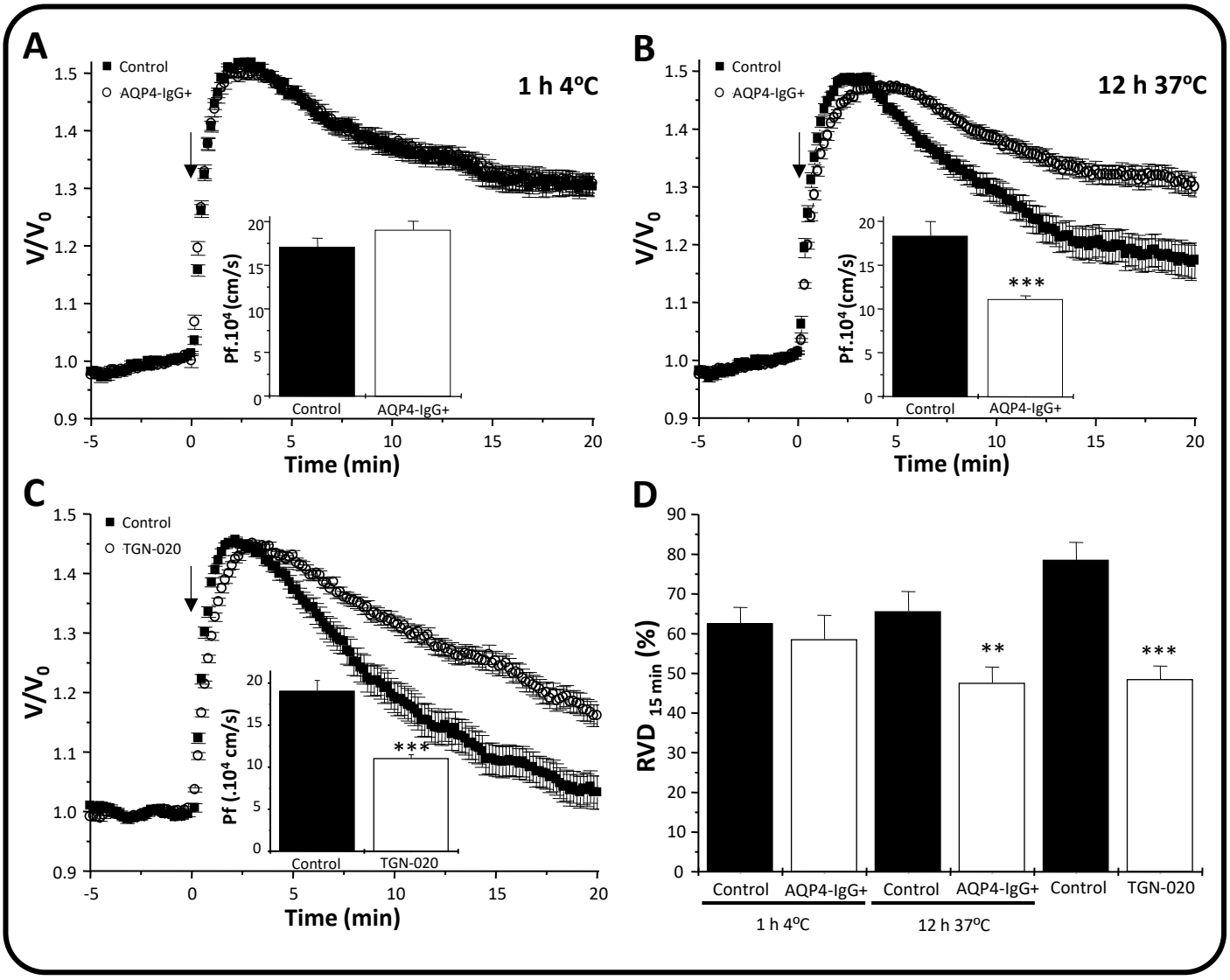

Figure 3: Osmotic water permeability and RVD response of MIO-M1 cells after exposure to control or AQP4-IgG positive sera. A-B: Time course of the relative cell volume (V/V_0) after exposure of cells to a hypoosmotic gradient (ΔOsM = 100 mOsM, indicated by arrows) in MIO-M1 cells treated with control or AQP4-IgG sera for 1 hour at 4°C (**A**) and for 12 hours at 37°C (**B**) or in the presence of AQP4 inhibitor TGN-020 100 nM or its vehicle (control) (**C**). Inserts show the osmotic water permeability (Pf) estimated from the time course of V/V_0 during the first 2 minutes after the hypotonic shock in both experimental conditions. Values are expressed as mean ± S.E.M. from 48-58 cells of 4-5 experiments, ***p<0.001, control serum vs. AQP4-IgG positive serum; *** p<0.0001 control vs. TGN-020. **D:** MIO-M1 cells RVD response 15 minutes after the maximal osmotic swelling (% $RVD_{15\ min}$) in all experimental conditions. Values are expressed as mean ± SEM from 48-58 cells of 4-5 experiments; **p<0.01, control serum vs. AQP4-IgG positive serum; *** p<0.0001 control vs. TGN-020.

Figure 4

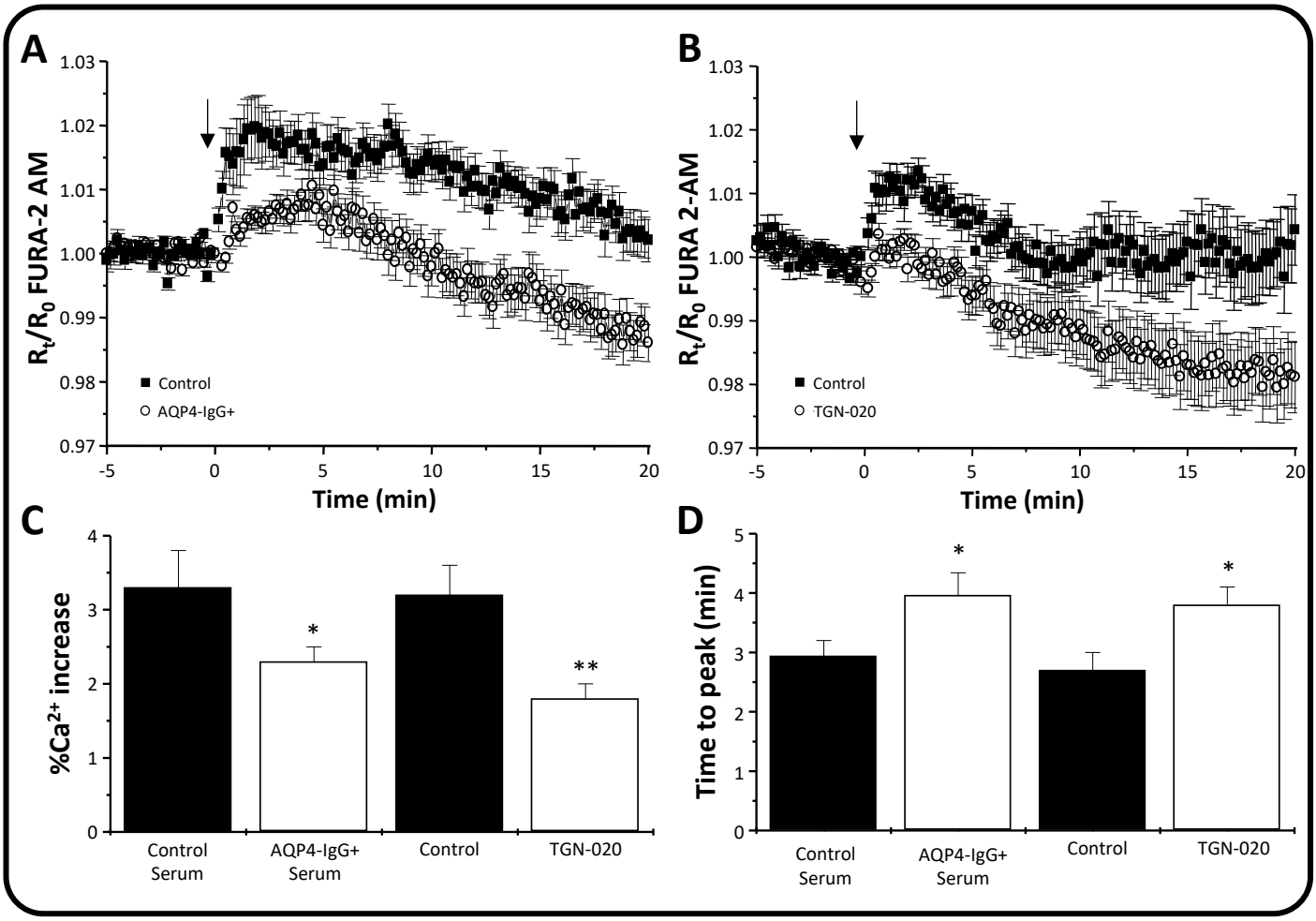

Figure 4: Changes in intracellular calcium levels during hypotonic shock and RVD in Müller cells after exposure to control or APQ4-IgG positive sera.

Cells were treated for 12 hours at 37°C with control or AQP4-IgG sera (**A**) or AQP4 inhibitor TGN-020 100 nM or its vehicle (control) (**B**). Then they were loaded with FURA-2 AM to measure intracellular calcium levels and exposed to a hypoosmotic gradient (ΔOsM = 100 mOsM, indicated by arrows). **A-B:** Kinetics of intracellular Ca^{2+} levels measured as the ratio 358/380 (R_t/R_0 FURA-2 AM). **C:** Maximal change in Ca^{2+} increase (%). **D:** Time to peak (min). Values are expressed as mean ± SEM for 45-53 cells from 4-5 independent experiments; *p<0.05 control serum vs. AQP4-IgG positive serum/TGN-020; ** p<0.01 control vs. TGN-020.

Figure 5

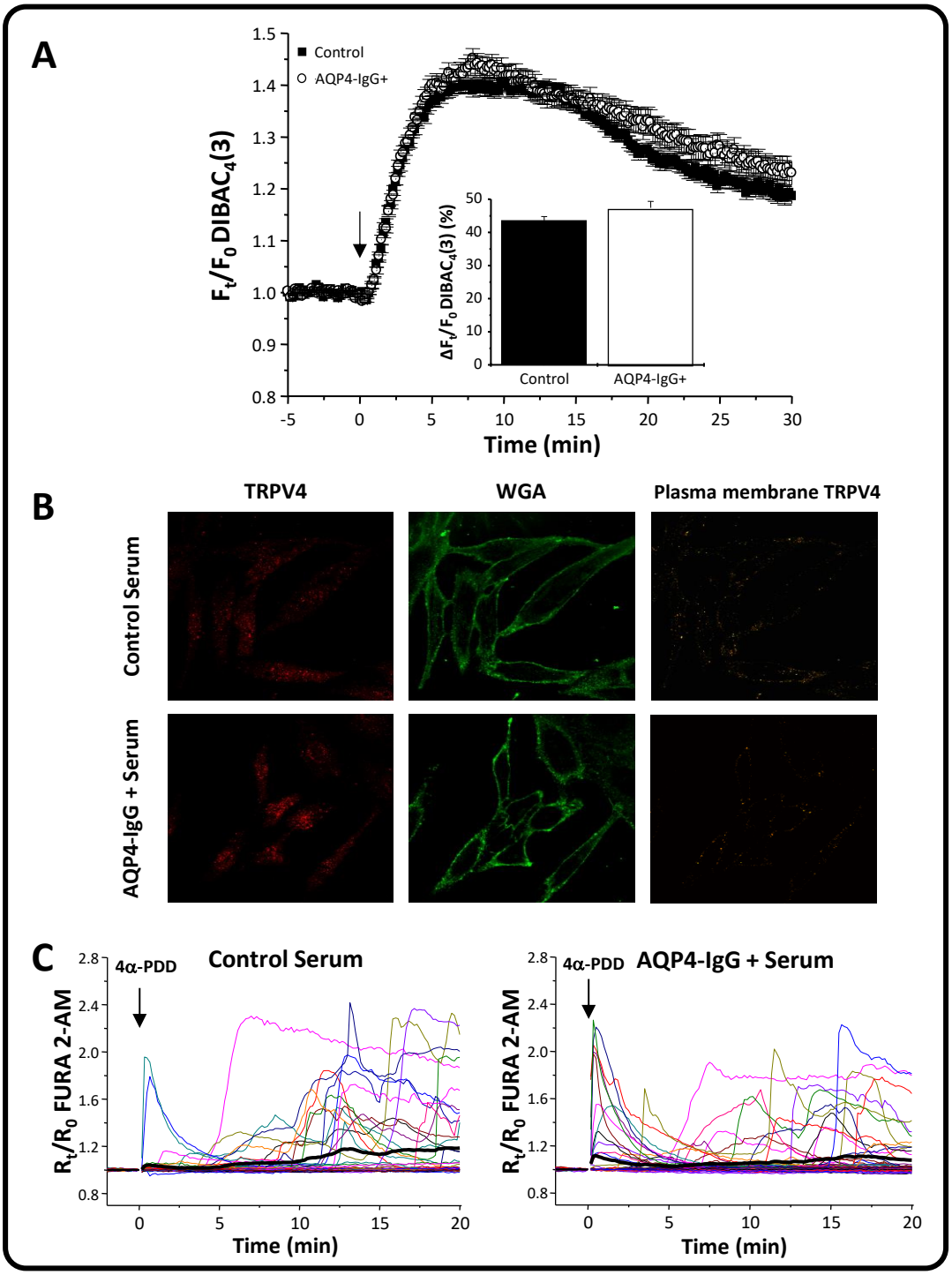
A
Control
AQP4-IgG+
F_t/F_0 DIBAC$_4$(3)
Time (min)
$\Delta F_t/F_0$ DIBAC$_4$(3) (%)
Control
AQP4-IgG+
B
TRPV4
WGA
Plasma membrane TRPV4
Control Serum
AQP4-IgG + Serum
C
4α-PDD
Control Serum
AQP4-IgG + Serum
R_t/R_0 FURA 2-AM
Time (min)

Figure 5: Changes in membrane potential during hypotonic shock and TRPV4 expression and function of MIO-M1 cells after exposure to control or APQ4-IgG positive sera.

A: Kinetics of $DIBAC_4(3)$ relative fluorescence (F_t/F_0). Cells were loaded with $DIBAC_4(3)$ to measure membrane potential and then exposed to a hypoosmotic gradient (ΔOsM = 100 mOsM, indicated by arrows). Inserts show the maximal change in maximum F_t/F_0 $DIBAC_4(3)$. Values are expressed as mean ± SEM for 42-57 cells from 4-5 independent experiments. **B:** Immunoflurescence confocal images of MIO-M1 cells stained with a polyclonal anti-TRPV4 antibody (red), WGA plasma membrane staining (green) and plasma membrane TRPV4 (yellow) after treatment for 12 hours at 37°C with control (left) or AQP4-IgG sera (right). Images are representative of three independent experiments. **C:** Kinetics of intracellular Ca^{2+} levels measured as the ratio 358/380 (R_t/R_0 FURA-2 AM) of MIO-M1 cells measured before and after specific TRPV4 activation with 10 µM 4α-PDD (indicated by arrows) in isotonic conditions in cells pretreated with control (top) or AQP4-IgG sera (bottom) for 12 hours at 37°C.

Figure 6

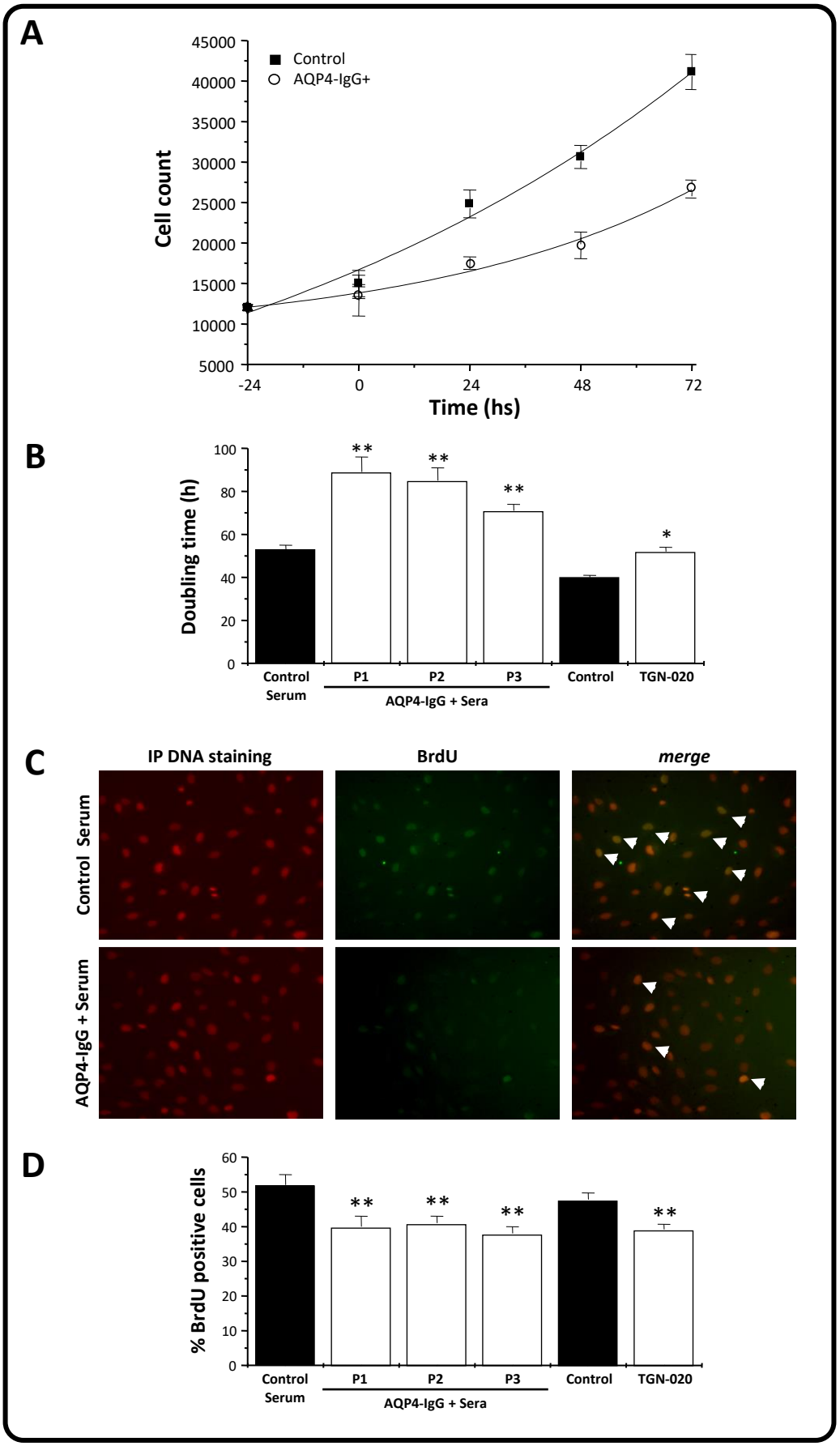
A
Control
AQP4-IgG+
Cell count
Time (hs)
B
Doubling time (h)
Control Serum
P1
P2
P3
AQP4-IgG + Sera
Control
TGN-020
C
IP DNA staining
BrdU
merge
Control Serum
AQP4-IgG + Serum
D
% BrdU positive cells
Control Serum
P1
P2
P3
AQP4-IgG + Sera
Control
TGN-020

Figure 6. Cell proliferation of MIO-M1 cells after exposure to control or APQ4-IgG positive sera. A-B: Growth kinetics of MIO-M1 cells determined by hemocytometry (**A**) and cell doubling time (**B**) obtained after fitting the individual experimental curves to exponential function and cell viability was assessed by Tripan Blue exclusion method. AQP4 inhibition by TGN-020 was also tested. Values are expressed as mean ± SEM, n=4 experiments for each condition; ** $p<0.01$ control serum vs. AQP4-IgG positive sera; *$p<0.05$ control vs. TGN-020. **C:** Representative images of proliferating MIO-M1 cells. The red channel shows propidium iodide (IP) DNA staining and the green channel shows the thymidine analog 5-Bromodeoxyuridin (BrdU) staining. Proliferating cells are indicated by white arrows. **D:** Percentage of BrdU positive cells in the presence of control or AQP4-IgG positive sera 1, 2 and 3 evaluated by immunocitochemistry. Values are expressed as mean ± SEM, n = 3 experiments for each condition; ** $p<0,005$ control vs. AQP4-IgG positive sera or control vs. TGN-020.

Figure 7

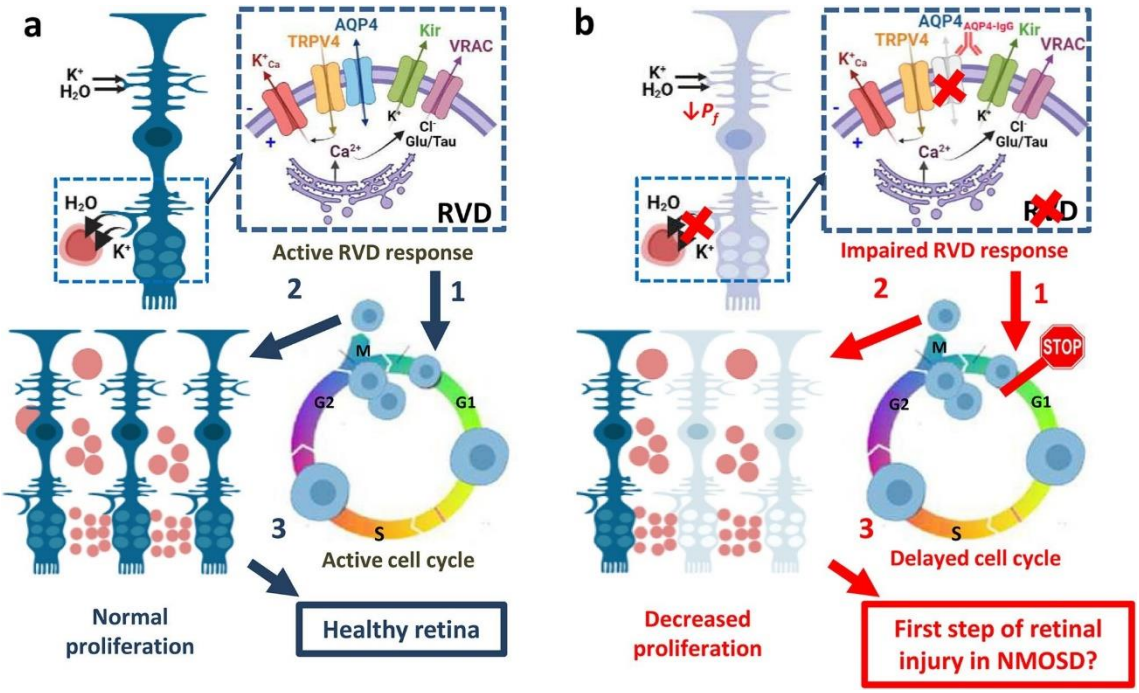

Figure 7: Proposed model to explain the complement-independent dis- function of Müller cells after AQP4-IgG binding to AQP4.

A: In phys- iological conditions, neural activity induces water and K+ uptake and cell swelling, which is followed by RVD response. RVD is a com- plex mechanism that involves AQP4 and TRPV4-dependent changes in membrane potential (Vm) as well as the activation of K+ and Cl– channels and the release of Taurine (Tau) and Glutamate (Glu) via VRAC (left upper panel). RVD capacity is also actively modulated during G0/G1 phase of cell cycle and plays an important role in cell cycle progress (1) to promote cell proliferation (2) and maintain retinal homeostasis (3).

B: In the presence of AQP4-IgG in NMOSD, AQP4 is partially removed from the plasma membrane and the acti- vation of the AQP4-dependent RVD response is affected, resulting in Müller cells' disfunction (right upper panel). Consequently, cell cycle is delayed (1) and the rate of cell proliferation decreases (2), probably contributing to the physiopathology of NMOSD in the retina (3)